A MAGNETICALLY SUSPENDED WHEEL FOR A MINIATURE GYRO MADE USING PLANAR FABRICATION TECHNOLOGIES*

Charles R. Dauwalter
Milli Sensor Systems and Actuators, Inc.
West Newton, MA

SUMMARY

The technical feasibility of a magnetically suspended rotating wheel for miniature gyro applications was investigated under a NASA SBIR contract. A concept for a configuration for a system of compact, lightweight magnetic actuators capable of generating the necessary suspension forces and fabrication using millimachining planar fabrication technologies was developed. Both capacitive and electromagnetic position sensing concepts were developed for implementing a closed loop control system for supporting the wheel. A finite difference technique, implemented in a spreadsheet environment, for analyzing the force characteristics of the actuator was used and the results verified with Finite Element Analysis.

INTRODUCTION

Electrostatic actuators have been widely studied and applied to microfabricated devices, not only because of their relatively simple fabrication requirements (due to their planar nature), but because in micro-sized devices, where very small gaps are practical, their maximum force capability can be higher than for magnetic devices. However, for devices in the centimeter size range, magnetic actuators are the only real choice. Our group is pursuing the development of inertial instruments, such as gyros and accelerometers, that can be fabricated through the use of many of the technologies widely used for micro-devices, but adapted for application to larger devices. We have termed these fabrication technologies "millimachining"; they are briefly discussed below. Consequently, we chose to investigate the application of magnetic suspension techniques for the support of a spinning wheel that can function as the angular momentum generator of a gyro. The basic wheel configuration we considered was a disk approximately 1 centimeter diameter and of the order of one to several millimeters thick. Several types of motor were initially considered to drive the wheel into rotation, including permanent magnet, hysteresis and reluctance types but, because of the unavailability of suitable materials that we were confident could be fabricated by the millimachining techniques we intended to exploit, we settled on a reluctance motor, of the type investigated by Ahn and Allen[1], having the required rotor features on the rim of the wheel, leaving most of the face areas of the disk for the magnetic suspension actuators and position sensors. The motor will not be discussed further in this paper.

* The majority of the work described was supported by NASA SBIR Contract NAS 7-1340

The proposed magnetic suspension system is expected to implement active control of the actuators by feedback of position information generated by suitable sensors; the actuators themselves can provide the sensing function also, if a time sharing mode of operation is utilized. Otherwise, separate electromagnetic sensors could be used, but these require the allocation of some of the volume that could otherwise be used to improve the forcing performance. A third reasonable option is capacitive sensing which is planar in nature and can be implemented in much less additional volume than separate electromagnetic sensors. Completely passive suspension control, without independent position sensors or control loops, is possible and has found wide use in floated inertial instruments developed at Draper Laboratory[2], but is not seen as practical for the spinning wheel at this time due to the lack of a practical passive method for providing damping to stabilize operation.

MILLIMACHINING

Millimachining is a design philosophy and fabrication approach that MSSA is developing from a merging of the traditional technologies and the emerging micro-machining technology, and applying it to devices in the size range between macro and micro. Millimachined inertial instruments are expected to realize higher performance than micro instruments due to larger angular momentum. Millimachined devices can also be expected to be less expensive and more reliable than conventionally fabricated macro-sized instruments because they can take advantage of the economy and reproducibility of batch processing and dispense with most of the expensive, time consuming and unreliable hands-on human labor. Millimachining, as we use the term, subsumes applicable portions of traditional macromachining with those from the emerging micromachining field into an effective and efficient technology for designing and manufacturing milli-sized instruments.

The approach we are pursuing in the development of millimachined instruments is to reduce well-understood three-dimensional traditional components to pseudo-two dimensional planar configurations with equivalent or better functionality. Complete instruments then become multi-layered in form and may be assembled simply and automatically by stacking and bonding the layers. The individual layers, each containing components for a number of instruments, are batch fabricated, tested if necessary, and finally stacked into a complete block containing many instruments, which can then be separated into individual ones.

MAGNETIC SUSPENSION ACTUATOR CONFIGURATIONS

Once the rim of the wheel had been allocated to the motor function, it was necessary to identify an efficient way to provide magnetic forces in the plane of the wheel as well as normal to it. Magnetic actuators capable of developing independently controllable forces in two orthogonal directions simultaneously were the subject of research in the mid-1970s for application to magnetically levitated high speed ground transportation systems[3] and we selected a variation of that idea for further development. Figure 1a shows a cross sectional view of a magnetically suspended wheel employing actuators of conventional construction which can simultaneously develop both vertical and horizontal forces; only half of the wheel system is

shown, the other half to the left of the centerline is a mirror image of the illustrated right-hand side. Each of the actuators is pie-shaped in form, occupying a quadrant of space, and has a number of concentric circumferential slots on both the stator and wheel portions to provide both normal and tangential forces; this is illustrated more clearly in Figure 3.

The relative dimensions illustrated in Figure 1a are approximately correct; the stator back iron width, b, and the rotor back iron width, d, must be approximately 4 times the tooth width, since (neglecting leakage) they carry the flux of 4 teeth. Dimension c is greater than b to provide space for the coil, which can either be wound around the back iron, as shown, or around the actuator stator legs above the teeth.

IMPROVED ACTUATOR CONFIGURATION

Figure 1b shows an actuator configuration (patent applied for) that was developed during this work and which, because of its essentially planar geometry, lends itself well to millimachining fabrication. It offers exactly the same functionality as the conventional construction illustrated in Figure 1a, but with significant functional and fabrication advantages for implementing a magnetically suspended wheel system. Since both actuator configurations illustrated have the same number of teeth and slots, and the same surface area, the maximum attainable tooth saturation limited force is approximately the same for each. However, the volume of iron, and thus weight, of both the stator and rotor structures is very much less for the planar actuator in Figure 1b than for the conventional construction in Figure 1a. This is made possible by distributing the exciting electrical conductors in the slots of the planar stator sections that were provided to enable tangential force generation, rather than winding them around the back iron or stator legs. As was the case for Figure 1a, the relative dimensions in Figure 1b are approximately correct. Dimensions b', the stator back iron thickness, and d', the rotor back iron thickness, are approximately half of dimension a', the tooth width, because each carries half of the tooth flux. Figure 2 is an enlarged section view of the planar actuator showing the conductor insulation; it should be apparent that, with the same fabrication process, the single conductor per slot could be subdivided into a number of conductors insulated from each other and the stator core to reduce the required excitation current.

WHEEL MAGNETIC SUSPENSION SYSTEM

The integration of the actuators described above into a complete magnetic suspension system for the spinning wheel is shown in Figure 3. The upper half of the figure depicts an assembly of the eight stator actuator sectors, four on each side of the wheel, that are required to implement the magnetic suspension of the wheel; in the lower half of the Figure, the four actuator sections on one side of the wheel have been rotated away from the wheel as a unit to expose the circumferential grooves on the wheel and the conductors embedded in the slots of the stator segments.

x and y axis forces: The magnetic forces generated by the actuator sections can be independently controlled, to provide complete three-dimensional suspension as follows; Figure 4 will be helpful in

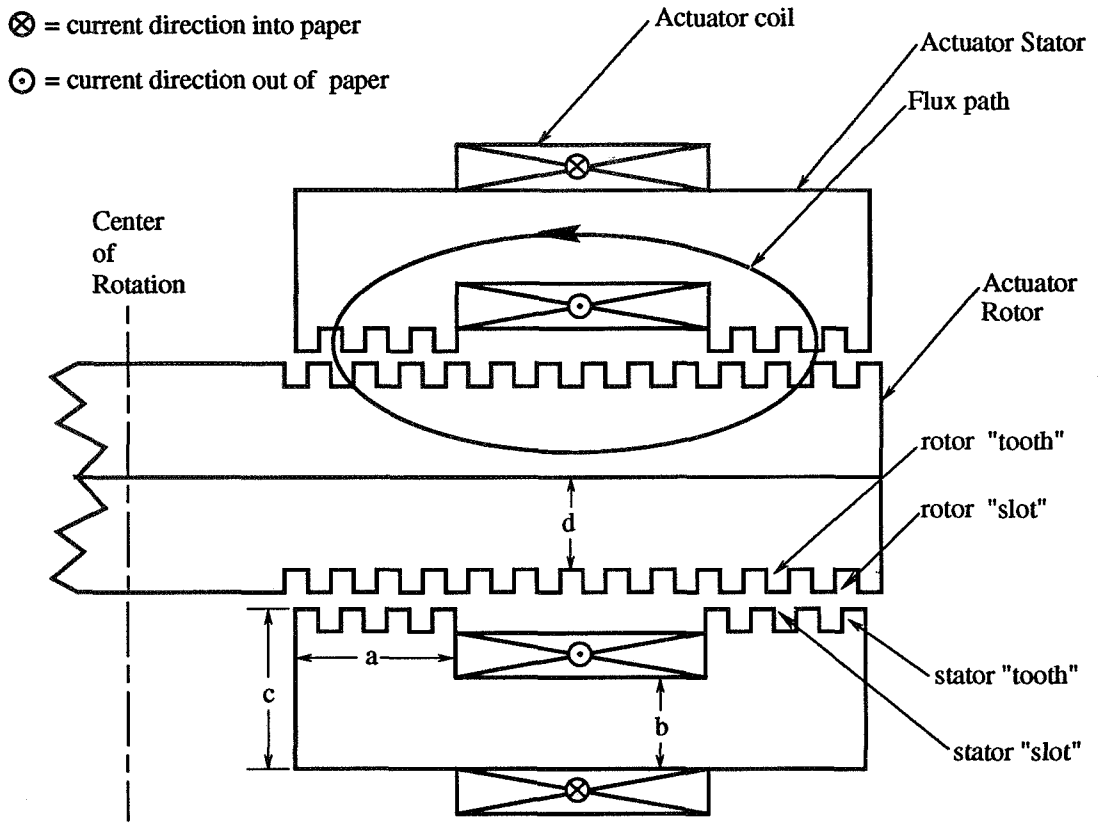

(a) Conventional Actuator

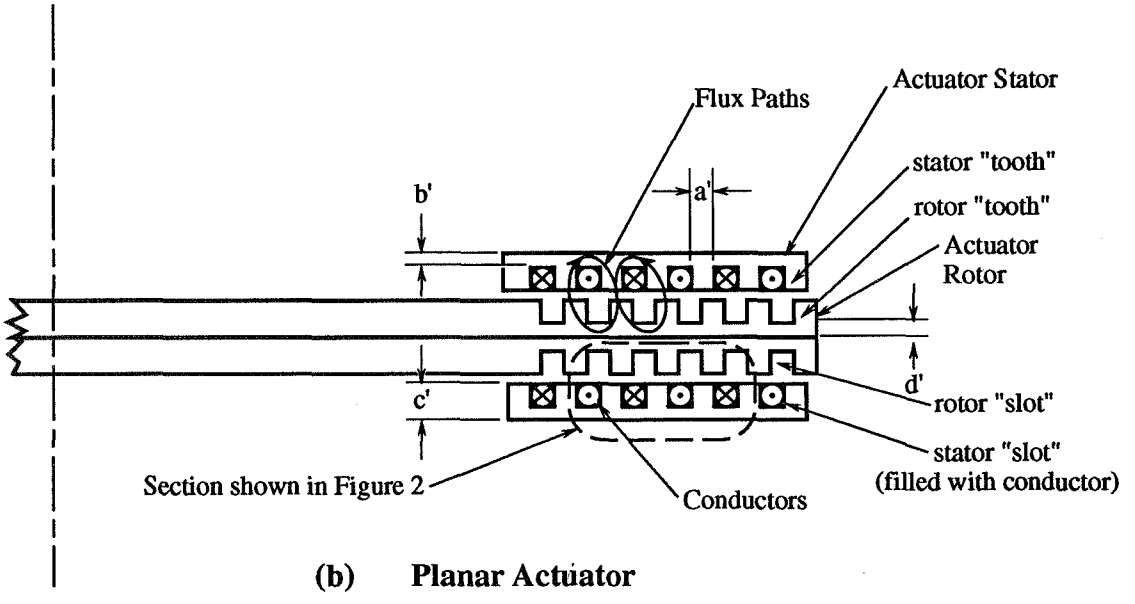

(b) Planar Actuator

Figure 1 Conventional and Planar Actuators

understanding the operational concept. First, a selected quiescent, or bias, current is passed through all of the conductors, creating essentially identical forces in each actuator sector; the z direction attractive force

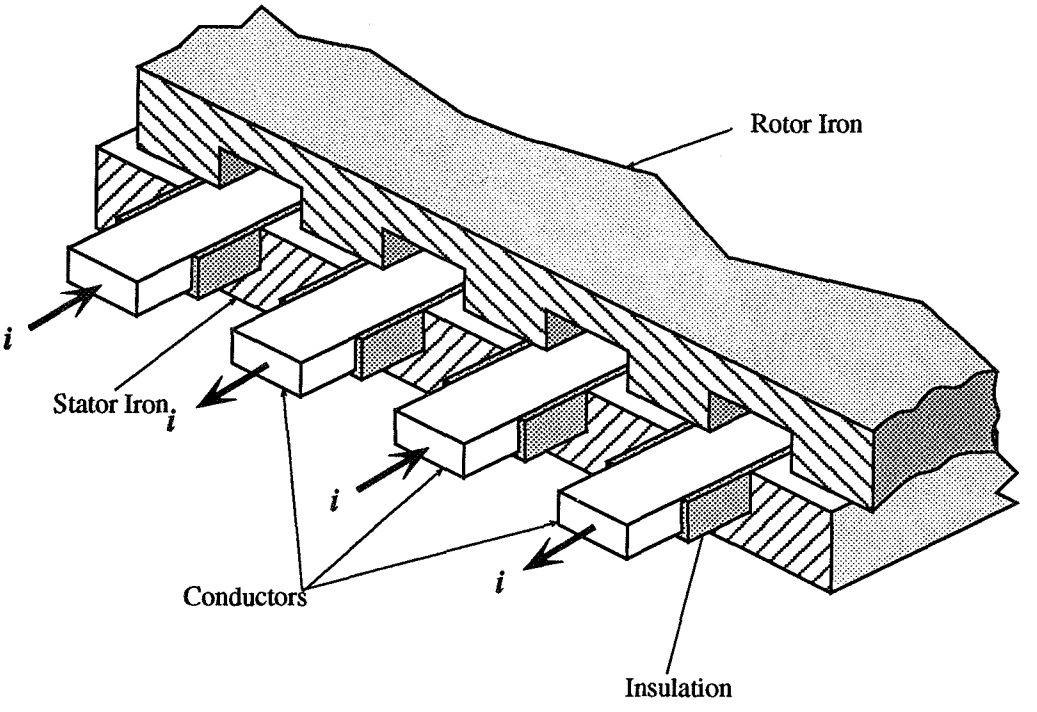

Figure 2 Enlarged View of Planar Actuator

of the actuator labeled B_{top} is equal to, but opposite in sign, that of the actuator labeled B_{bottom} while the x forces are equal and in the same direction (-x direction). The +z direction attractive force of the actuator, labeled D_{top}, is equal to, but opposite in sign, that of the actuator D_{bottom}, while the x forces are equal and in the same direction (+x direction). Thus, no net force is developed on the rotor. A similar situation applies to the y-axis forces. +x-axis force only, without affecting the other forces and moments, is generated by increasing the current in the actuator conductors of, D_{top} and D_{bottom}, by Δi and decreasing that in the conductors of B_{top} and B_{bottom} by Δi. y-axis forces are generated in a similar fashion.

z-axis forces: +z-axis force only, without affecting the other forces and moments, is generated by increasing the current in the conductors of actuator sectors A_{top}, B_{top}, C_{top} and D_{top}, by an amount Δi, while decreasing the current in the conductors of A_{bottom}, B_{bottom}, C_{bottom} and D_{bottom}, by Δi; the net x and y-axis forces and moments are unchanged.

Moments about x- and y-axes: Counterclockwise torque on the rotor, $+M_x$, about the x-axis is generated by increasing the current in the conductors of A_{top} and C_{bottom} by Δi and decreasing the current in the conductors of A_{bottom} and C_{top} by Δi; the x, y and z forces are unchanged. Clockwise torque on the rotor, $-M_x$, is generated by decreasing the current in the A_{top} and C_{bottom} conductors by Δi and increasing the current in the A_{bottom} and C_{top} conductors by Δi; the x, y and z forces are again unchanged. Torques about the y-axis are generated similarly.

The control logic is summarized in Table 1. In addition to making independent control of the forces and torques possible, the bias current provides the benefit of linearizing the force vs. control current relationship, which would otherwise be quadratic.

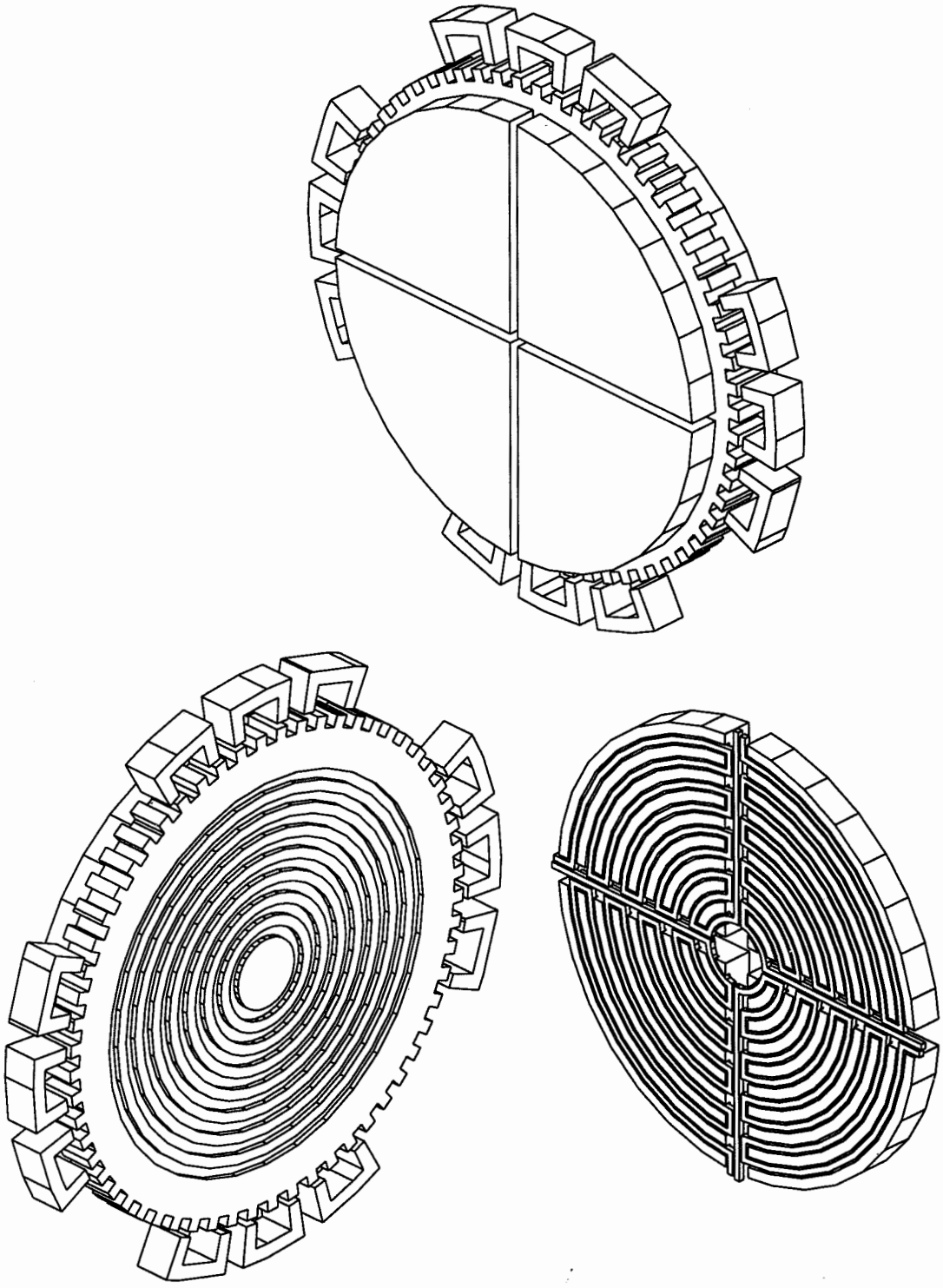

Figure 3 Assembled Magnetic Suspension Stator Sectors And Gyro Wheel

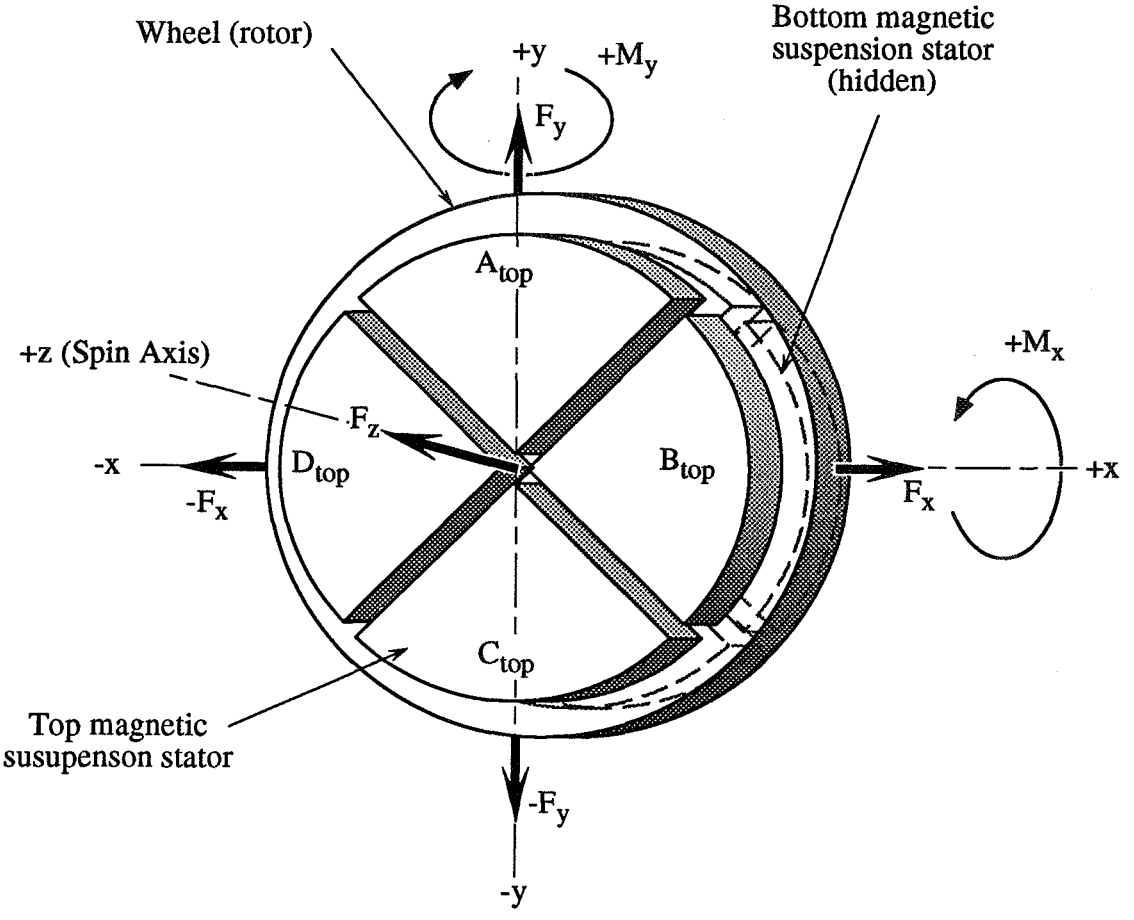

Figure 4 Magnetically Suspended Wheel

Table 1 Magnetic Suspension Control Logic

Sector	$+F_x$	$-F_x$	$+F_y$	$-F_y$	$+F_z$	$-F_z$	$+M_x$	$-M_x$	$+M_y$	$-M_y$
A_{top}	$+\Delta i$	$-\Delta i$	$+\Delta i$	$-\Delta i$	$+\Delta i$	$-\Delta i$	$+\Delta i$	$-\Delta i$		
B_{top}					$+\Delta i$	$-\Delta i$			$-\Delta i$	$+\Delta i$
C_{top}			$-\Delta i$	$+\Delta i$	$+\Delta i$	$-\Delta i$	$-\Delta i$	$+\Delta i$		
D_{top}	$-\Delta i$	$+\Delta i$			$+\Delta i$	$-\Delta i$			$+\Delta i$	$-\Delta i$
A_{bottom}			$+\Delta i$	$-\Delta i$	$-\Delta i$	$+\Delta i$	$-\Delta i$	$+\Delta i$		
B_{bottom}	$+\Delta i$	$-\Delta i$			$-\Delta i$	$+\Delta i$			$+\Delta i$	$-\Delta i$
C_{bottom}			$-\Delta i$	$+\Delta i$	$-\Delta i$	$+\Delta i$	$+\Delta i$	$-\Delta i$		
D_{bottom}	$-\Delta i$	$+\Delta i$			$-\Delta i$	$+\Delta i$			$-\Delta i$	$+\Delta i$

POSITION SENSING APPROACHES

Practical approaches to implementing the position indication needed for an active suspension control system can be described only briefly here, due to space limitations; they are described in considerable detail in the contract Final Report. Briefly, four techniques for position sensing were explored, one using the variation of capacitance with position of capacitors fabricated on the tips of the stator teeth and three using the variation of the stator segments' inductance with position: 1) adding capacitor electrodes to the actuator stator structure to implement capacitive position sensing, as schematically illustrated in Figure 5, 2) continuously sensing the inductance of the actuators while they are being used to generate force and 3) periodically time sharing the actuators so that they are used for forcing for a part of the period and then as sensors for the balance of the period; the latter reduces the maximum force that could be developed, 4) sharing the space allocated to the sensor and actuator stators, providing a portion for forcing and using the balance for sensing. This, like time sharing, would also decrease the maximum force, but might be practical for situations not requiring maximum force capability, and it would reduce the effect of the interaction of magnetic material nonlinearities and forcing current variations on accuracy of position sensing.

The actuators themselves can be effectively used for sensing the position of the rotor because their self-inductances change with both tangential and normal motion; an output voltage proportional to change in inductance, and thus in position, results when the actuators are used in a suitable bridge circuit. The sensing sensitivity will be maximum when the geometry is selected for maximum developed force because both position sensing sensitivity and the developed force are directly proportional to the rate of change of inductance with position.

All of the position sensing approaches described above provide ideal collocation of the sensing and forcing functions, avoiding the control system complications caused by non collocation.

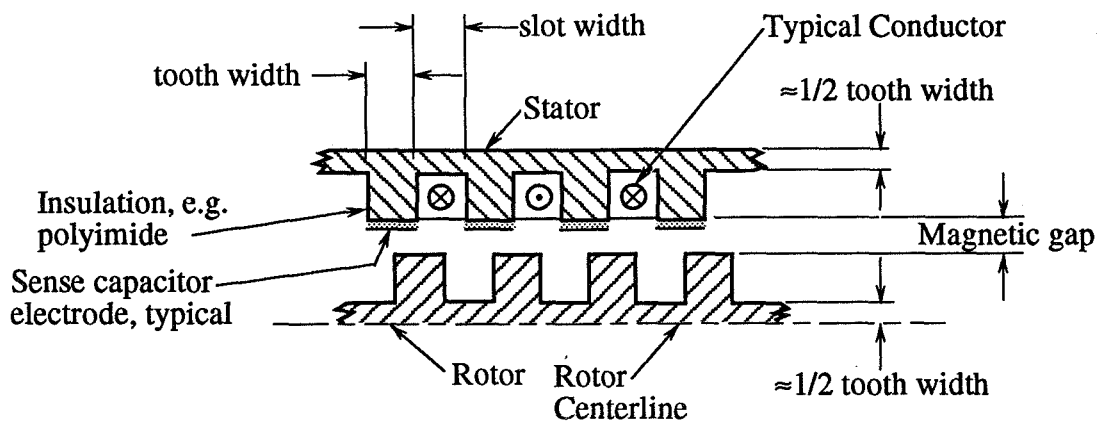

Figure 5 Actuator With Position Sensing Capacitors

Zero Current Regions

In a region devoid of electric currents, the magnetic field can be derived from a magnetic scalar potential Φ:

$$\overline{H} = -\overline{\nabla}\Phi \tag{1}$$

where Φ satisfies Laplace's equation

$$\nabla^2\Phi = 0 \tag{2}$$

In the two dimensional case considered here,

$$\overline{B_x} = \mu_0 \overline{H_x} = -\mu_0 \frac{\partial \Phi}{\partial x} \text{ and } \overline{B_y} = \mu_0 \overline{H_y} = -\mu_0 \frac{\partial \Phi}{\partial y} \tag{3a, 3b}$$

Non-Zero Current Regions

In a region containing electric currents, the scalar potential formulation is invalid; the magnetic field can be obtained from a magnetic vector potential $\overline{A}$:

$$\overline{B} = \overline{\nabla} \times \overline{A} \tag{4}$$

where $\overline{A}$ satisfies Poisson's equation

$$\nabla^2 \overline{A} = -\mu_0 \overline{J} \tag{5}$$

In the two dimensional cases considered here, $\overline{J}$ and $\overline{A}$ have only a z component, perpendicular to the x-y plane, with the result that

$$B_x = \frac{\partial \overline{A}}{\partial y} \text{ and } B_y = -\frac{\partial \overline{A}}{\partial x} \tag{6a, 6b}$$

The Finite Element Method has been highly developed for the analysis of magnetic field problems, and a number of programs are commercially available for that purpose; some, such as ANSYS, as a subset of a more general purpose package for engineering analysis. While these programs are now very sophisticated and have excellent capabilities, they are generally expensive, making them difficult to afford for very small organizations and individuals. Also, because of their broad capabilities, they tend to be rather complex, requiring substantial familiarization efforts by the user. Finite difference approximations to Laplace's and Poisson's equations can be used in conjunction with widely available spreadsheet programs, such as Excel® for useful analysis of a limited class of magnetic analysis problems, which includes the actuator discussed here. Since many engineers already have spreadsheet programs and use them extensively for engineering analysis, cost is not an impediment, and the simple nature of the procedures requires negligible effort for familiarization with their use.

Finite Difference Approximations of Laplace's and Poisson's Equations

If a discretized square coordinate grid is superimposed on the problem region with a grid spacing of $\Delta x=\Delta y$, then Laplace's equation in two dimensions can be approximated[4] by

$$\phi_1 + \phi_2 + \phi_3 + \phi_4 - 4\phi_0 \cong 0 \tag{7}$$

with the result that

$$\phi_0 = \frac{1}{4}\left(\phi_1 + \phi_2 + \phi_3 + \phi_4\right) \tag{8}$$

where ϕ_0 is the value of Φ at a particular node and ϕ_1, ϕ_2, ϕ_3, ϕ_4 are the values of Φ at the surrounding nodes. This simple equation is the basis for the field solutions using a spreadsheet; actually, the spreadsheet contains only this equation, repeated, and the relevant boundary conditions.

Similarly, Poisson's equation in two dimensions can be approximated by

$$\overline{A}_1 + \overline{A}_2 + \overline{A}_3 + \overline{A}_4 - 4\overline{A}_0 \cong -\mu_0 \overline{J} \tag{9}$$

with the result that

$$\overline{A}_0 = \mu_0 J + \frac{1}{4}\left(\overline{A}_1 + \overline{A}_2 + \overline{A}_3 + \overline{A}_4\right) \tag{10}$$

applies to those nodes of the problem region which contain currents; Equation (8) applies elsewhere.

Boundary Conditions

Four types of boundary conditions are applicable to the type of problem being discussed here. The first is the Dirichlet boundary condition in which a prescribed value of the potential function is applied to the boundary. The second is the Neumann boundary condition in which field is specified on the boundary; in this case, the field has no components normal to the boundary. The third consists of symmetry relationships; this type appears in problems, like the present one, in which the overall geometry consists of repeating sub-units. In this type, for example, the potential value at the first node to the left of the left-hand boundary is specified to be the same as the value at the first node to the left of the right-hand boundary and vice-versa. The field may have in this case components normal to the boundary. A fourth boundary condition, used in vector potential models where iron of infinite (or relatively high) permeability is assumed, is the specification that the normal derivative be zero. This results in zero field parallel to the iron surface, a consequence of the infinite permeability; in scalar potential models, this is a natural consequence of the Dirichlet boundary conditions used.

Force Calculations Using Maxwell's Stress Tensor

The Maxwell's stress tensor[5] can be used to obtain expressions for the normal stress, σ, and the shear stress, τ, on a differential surface area, ds, that is produced by the magnetic field, H, at that surface. These expressions provide a convenient and powerful method for calculating the magnetic forces exerted on a body, and are commonly used in finite element magnetics programs. If H_x and H_y are the magnetic field components parallel and normal, respectively, to the surface, ds, then the magnetic stresses on ds are

$$\tau = \mu_0 H_x H_y \tag{11}$$

and

$$\sigma = \frac{\mu_0}{2}\left(H_y^2 - H_x^2\right) \tag{12}$$

The total force and torque on a body are calculated by integrating the stresses along a closed contour in the space surrounding the body.

Solution Technique

The solution technique utilized for obtaining the potentials from which the fields are derived is a relaxation method, the Gauss-Seidel method. To implement this in a spreadsheet, the calculation option is set to allow iteration. With iteration enabled, recursive calculations are permitted; i.e., the equations for the calculations in a cell are allowed to contain parameters which depend upon the results of the calculation, e.g. x=x+1; without iteration enabled a "circular reference" error would result. A suitable limit on the number of iterations allowed is set, and a value for maximum change set. Then, the calculation proceeds until either the maximum number of iterations is reached, or the maximum change in the value of any cell for one cycle of calculations is less than the specified value. The accuracy of the result depends both upon the specified maximum change in cell value per iteration and the fineness of the subdivision of the problem region. The adequacy of the fineness of the net can be assessed by comparing the values of Φ for the problem with net spacing $\Delta x=\Delta y=h$ with the results with net spacings $\Delta x=\Delta y=h/2$. Karplus[6] describes a useful extrapolation which determines the potential distribution of a model with a mesh at least as fine as $\Delta x=\Delta y=h/4$:

$$\Phi_{\Delta x=\Delta y=h/4} = \Phi_{\Delta x=\Delta y=h/2} - \frac{1}{3}\left(\Phi_{\Delta x=\Delta y=h} - \Phi_{\Delta x=\Delta y=h/2}\right) \tag{13}$$

Typical Spreadsheet Implementing Finite Difference Equations

Figure 6 shows a typical spreadsheet set up to solve for the vector potential of a problem. The actuator configuration discussed in this paper is illustrated, but with a relatively small number of cells to permit the equations for the cells to be shown more clearly on the sheet. The

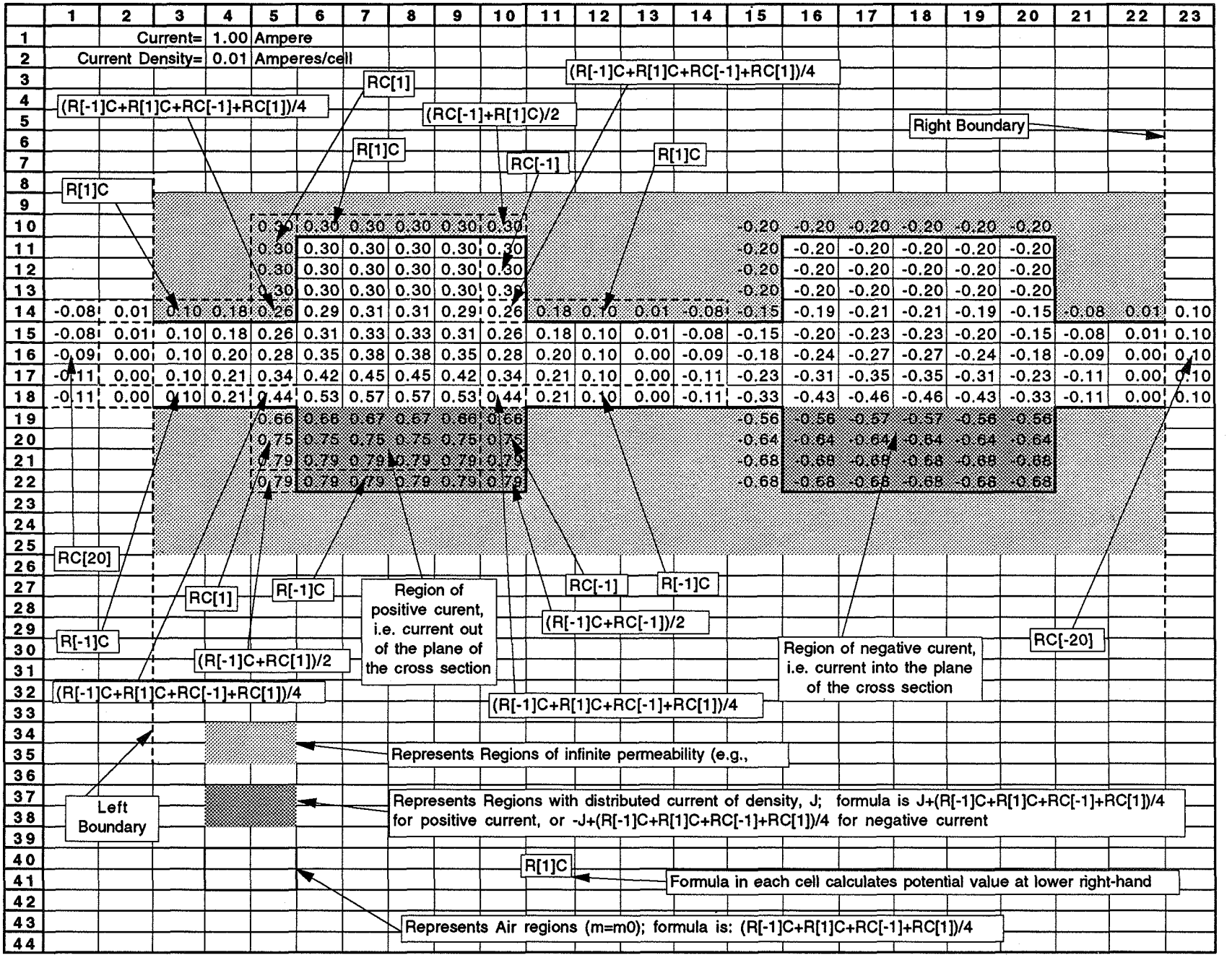

Figure 6 Example Spreadsheet Actuator Analysis

regions representing the iron and the current carrying conductors is shaded, as indicated by the key on the Figure, to facilitate ready visualization of the geometry being modeled; the boundary between the iron and air is indicated by a heavy black line. On the left-hand side of the sheet, cells containing the same equations are enclosed in dotted boxes; arrows connect those regions with the equations that they contain; this identification is omitted on the right side, except for the boundary condition. The intersections of the individual cell walls correspond to nodes of the square grid superimposed on the problem region to discretize it for finite difference analysis. The equation which an individual cell contains calculates the value of the node at its lower right-hand corner.

As discussed above, Equation (10) is implemented in all cells in regions where current is not zero, and Equation (8) in all other cells except at the boundaries. At the right and left-hand boundaries, the symmetry condition discussed above, under boundary conditions, is applied to reflect that the actuator consists of repeating sets of the basic configuration of two teeth and two slots. On the remaining boundaries, representing the iron portions of the actuator, the boundary values are set to equal those of the nearest adjacent non-boundary node, so that the normal derivative of the potential is zero; this reflects the effect of the assumed infinite permeability of the iron, which results in a zero value for the field gradient parallel to the boundary (i.e., the magnetic flux lines are normal to the boundary.) In the equations for the cells of regions containing current, j is the current density in the region.

Field Visualization

It is sometimes helpful in magnetics design problems to be able to visualize the field distribution; this may readily be done with the spreadsheet solution approach. Visualization is almost trivial for problems utilizing the vector potential formulation, since the magnetic field is parallel to equipotentials of $\overline{A}$, and many spreadsheet programs have a built-in facility for easily plotting equipotentials. This function is provided by the Contour Chart format of the 3-D Surface Chart type in Excel®. Producing a field plot is somewhat more involved for scalar potential problems, since the field lines are orthogonal to the equipotentials. If the problem is reformulated with the appropriate Dirichlet boundaries replaced by Neumann boundaries and vice versa, the desired result is obtained. For problems such as the configuration shown in Figure 1a, in which the stator and rotor surfaces are properly Dirichlet boundaries and the boundaries of the repeating element are the symmetry boundary described above, it is necessary for correct results to ensure that the problem is set up such that the symmetry boundaries are located in a region where the field lines are parallel to those boundaries. This requires some intuition and/or experience and is not possible, except very approximately, for some problems.

ANALYSIS RESULTS

The results of the analysis of the force characteristics of the planar actuator are shown in Figures 7 and 8, which show tangential and normal forces vs. tangential displacement for various air gap values. The forces indicated are those for the repeating unit of two teeth and two slots, per meter of actuator length. The configuration that was analyzed is the lower half of the planar

actuator illustrated in Figure 1b and Figure 2. Both the tooth and slot widths were 32 mm and the slot depth was 16 mm for the finite element analyses and 32 mm for the spreadsheet analysis. The purpose of the analyses was to provide an initial understanding of how the normal and tangential forces depend upon the design variables, in particular the air gap relative to the stator tooth and slot widths. No attempt was made to explore the effect of varying the tooth to slot width ratio to yield more optimum characteristics; such an optimization study will be appropriate for future work.

The maximum tangential force, for all air gaps in the range studied, occurs when the normal force is approximately half-way between its maximum and minimum values; since the tangential force, for the proportions studied, was always smaller than the normal force (by a factor of approximately 5), designs for applications would likely be chosen to operate in this region. It is considered likely that higher ratios of tangential to normal forces can be attained by modifying the ratio of the tooth to slot widths used, quite arbitrarily, in this study; the latter ratio is also important in influencing the power dissipation since making the slot wider allows a larger conductor cross-section area resulting in lower total resistance and power. Figure 9, which compares the results of the FEM and spreadsheet analyses for one value of air gap, demonstrates that the spreadsheet method of analysis produces predictions that are close, but not identical to those of the finite element analysis method. Some of the difference may be due to the assumption of infinite material permeability in the spreadsheet analysis (a permeability of 4,000 was assumed in the finite element analyses) and that the slot depth used for the FEM analysis that was half the value used for the spreadsheet analysis.

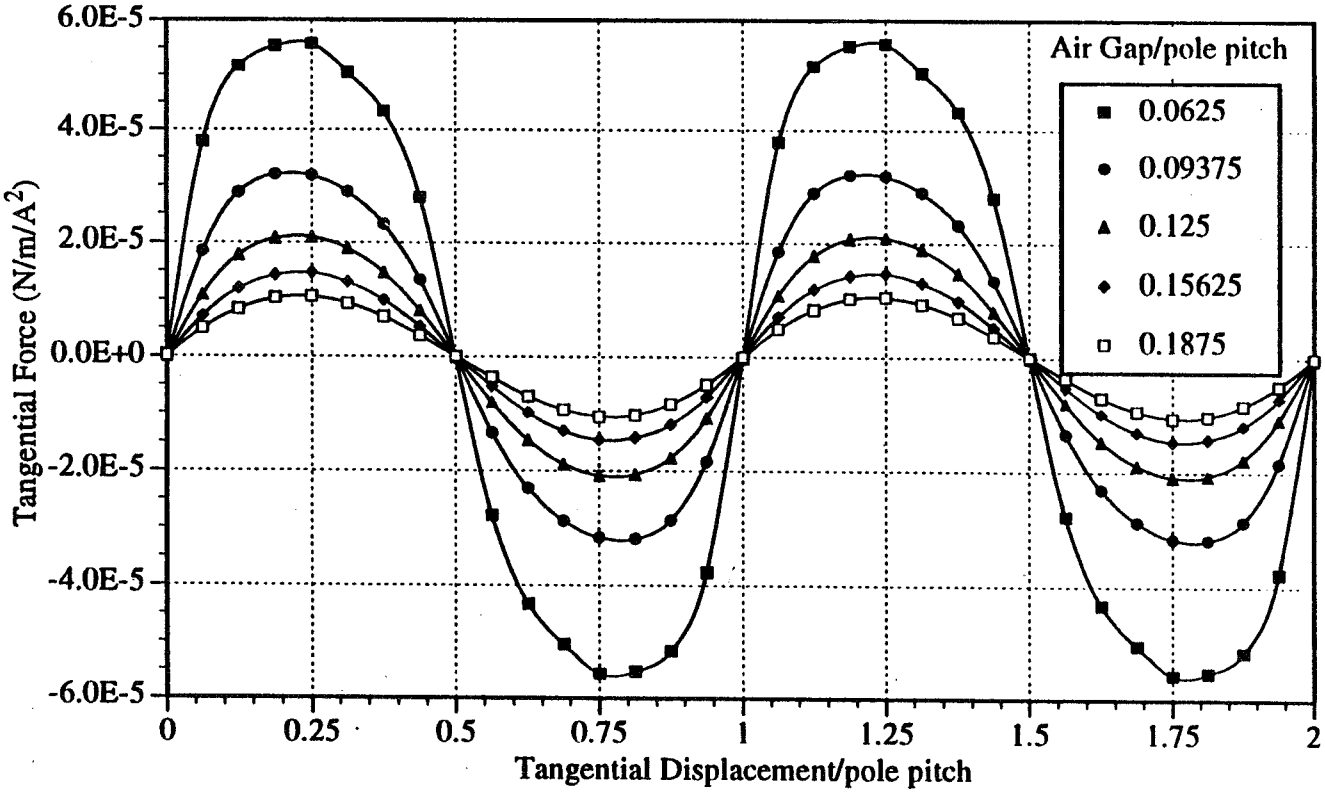

Figure 7 Tangential Force vs. Tangential Displacement and Air Gap, FEM

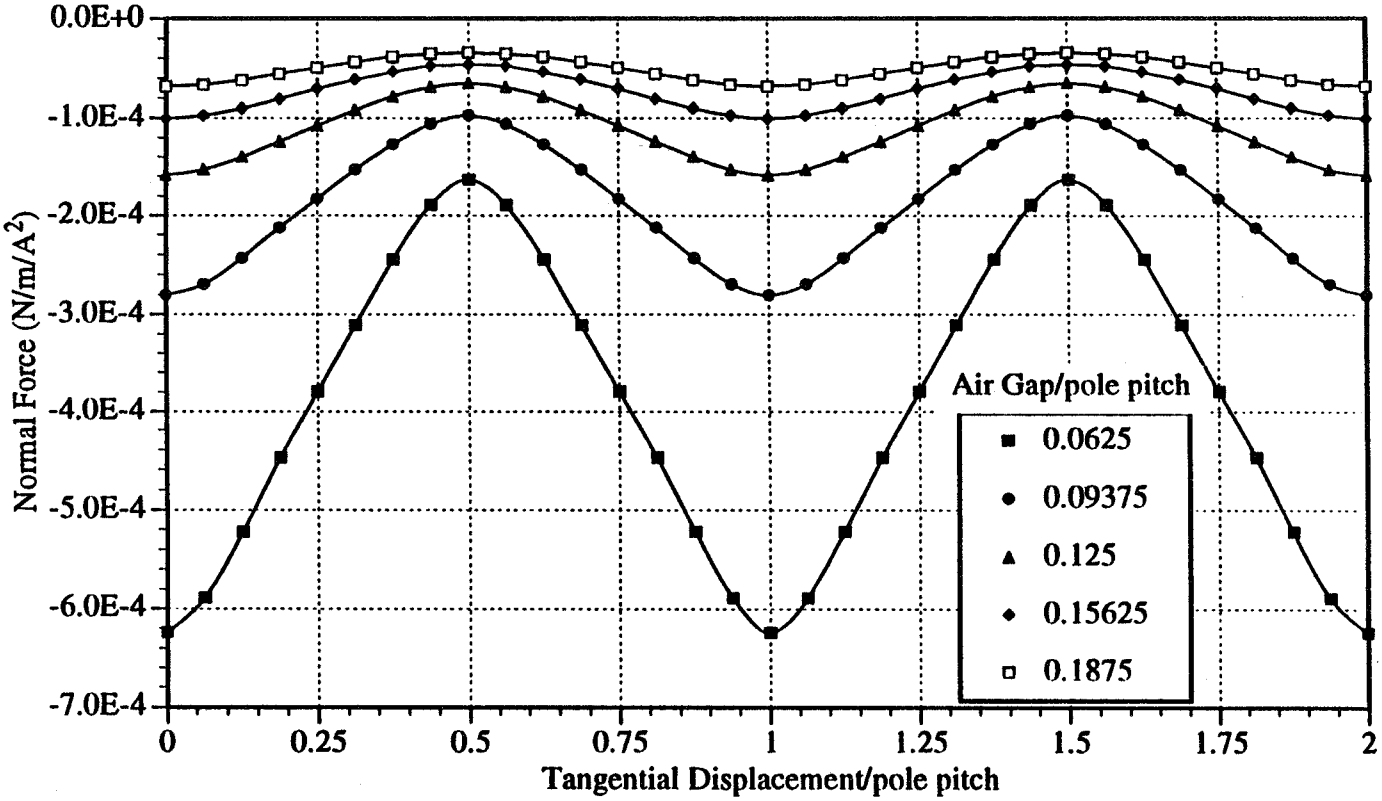

Figure 8 Normal Force vs. Tangential Displacement and Air gap, FEM

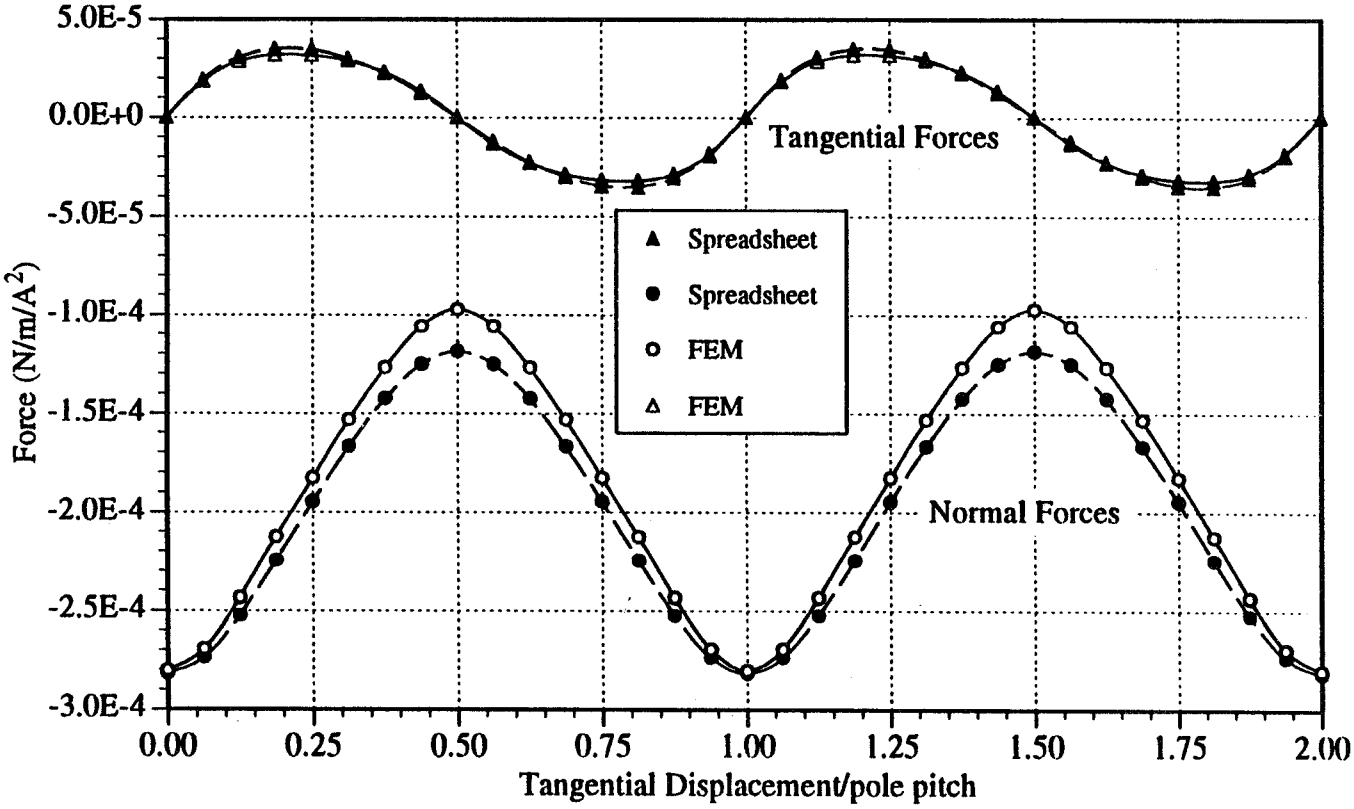

Figure 9 Spreadsheet/FEM Comparison: Force vs. Displacement

Conclusions

The work described established the technical feasibility of a magnetically suspended spinning wheel for applications such as a miniature gyro. The planar actuator configuration that was developed appears to be well suited to fabrication by millimachining processes as well as making lighter weight and more volume efficient actuator designs possible. The fabrication of the planar actuator was confirmed by supporting work at Georgia Institute of Technology, where it was possible to fabricate a proof-of-concept miniature actuator stator assembly in only a few weeks after the design was identified. Performance analysis of electromagnetic devices using finite difference approximations to the relevant field equations in a spreadsheet environment was shown to be a convenient and reasonably accurate alternative to finite element analysis programs, at least for relatively simple geometry's and for preliminary design purposes. Further work may improve the spreadsheet analysis capabilities, in particular permitting finite material permeability and axi-symmetric geometry's to be handled.

ACKNOWLEDGMENTS

The author gratefully acknowledges the assistance provided by the following: Dr. Randy Bartman, contract Technical Monitor at JPL, for support, encouragement, and helpful discussions of potential NASA applications of the technology, Dr. Raymond Carroll of MSSA for timely and helpful discussions of the field solutions, Kevin Hinckley and Joseph Nicolaisen of the Equipment Division of Dynamics Research Corp. for finite element analyses, and Prof. Mark G. Allen and his student, William P. Taylor, at Georgia Institute of Technology for their expert advice on actuator design considerations for millimachining fabrication and the fabrication of proof-of-concept devices.

REFERENCES

1. Ahn, C. H. and Allen, M. G.: A Fully Integrated Micromagnetic Actuator with Multilevel Meander Inductive Core. Proc. IEEE Solid State Sensor and Actuator Workshop, Hilton Head, SC, June 1993.

2. Frazier, R. H.; Gilinson, P. J., Jr.; and Oberbeck, G. A.: *Magnetic and Electric Suspensions.* MIT Press, Cambridge, MA, 1974, pp. 147 et seq.

3. Wormley, D. N, et. al: Noncontacting Suspension and Propulsion for Ground Transportation. Report DOR/RSPA/DPB-50/79/34, Department of Transportation, Research & Special Programs Administration, Washington, DC, 1979 (Available NTIS, Springfield, VA).

4. see, e.g., Karplus, W. J.: *Analog Simulation*, McGraw-Hill, New York, 1958, pg. 92-94.

5. Ida, Nathan and Bastos, Joao, P. A.: *Electromagnetics and Calculation of Fields*, Springer-Verlag, New York, 1992, pp. 188-195.

6. Karplus, *op. cit.*, pp. 200.